

TiO₂ Supported Pt Based Bimetallic Nanocatalysts for Selective Hydrogenation of Citral†

S. A. ANANTHAN, R. SURESH, K. GIRIBABU,
R. MANIGANDAN and V. NARAYANAN*

Department of Inorganic Chemistry, School of Chemical Sciences, University of Madras,
Guindy Campus, Chennai-600 025, India

vnnara@yahoo.co.in

Received 23 January 2013 / Accepted 15 February 2013

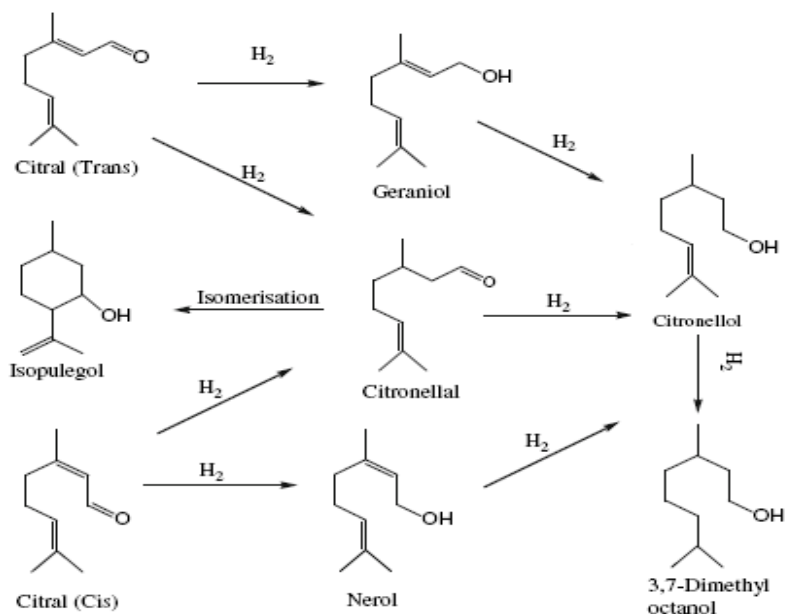
Abstract: TiO₂ supported Pt based bimetallic nanocatalysts were prepared by impregnation method and reduced at two different temperatures, 375 °C and 575 °C for the selective hydrogenation of citral to the corresponding unsaturated alcohols namely; geraniol (GOL) and nerol (NOL). The catalysts were characterized by BET surface area measurement, FT-IR, SEM, EDAX, TEM, XRD and XPS. The prepared nanocatalysts are uniformly dispersed with an average particles size 50-100 nm and zero valence metallic state. The SMSI (Strong Metal-Support Interaction) effect shows that the catalysts reduced at higher temperature leads to an increase in selectivity toward unsaturated alcohols (GOL & NOL) for Pt-Ru/TiO₂ compared to Pt-Pd/TiO₂ and Pt-Au/TiO₂ nanocatalysts. In addition a second metal (Ru) also leads to an increase of the GOL & NOL selectivity during the citral hydrogenation. The generated partially oxidized second metal species due to the difference in electronegativity, strongly binds the C=O group and also paves the way for the selective activation of the C=O bond. Metal support interaction and promoter active metal interaction increased the unsaturated alcohol formation.

Keywords: Bimetallic nanocatalysts, TiO₂ supported, SMSI effect, Thermal reduction, Citral hydrogenation, Unsaturated alcohols

Introduction

Selective hydrogenation of α,β -unsaturated aldehydes to their corresponding alcohols is major process of chemical industries, especially in the fine chemical industries¹⁻³, such as for the production of pharmaceuticals, detergents, cosmetics, flavors and fragrances^{4,5}. The reaction can lead to variety of products, the C=C double bond is hydrogenated to give a saturated aldehyde or the C=O double bond is involved, yielding an unsaturated alcohol and hydrogenation of both can occur resulting in a saturated alcohol and also formation of cyclization. Due to the fact that the C=C bond presents a lower binding energy than the C=O bond, the formation of saturated aldehydes is thermodynamically favored, decreasing the selectivity to the unsaturated alcohol⁶⁻¹⁰. In the present work, selective hydrogenation of citral (Scheme 1) was studied^{11,12}. Citral and its related unsaturated alcohols have considerable interest in the perfumery industries¹³⁻¹⁴.

†Presented to the National Conference on Chemistry Solutions at SRM University, India



Scheme 1. Reaction path way of citral hydrogenation

The hydrogenation reactions are generally catalyzed by transition metals of group VIII of the periodic table. However, the selectivity of these metals with relation to hydrogenation of C=O bond has shown itself specific for each metal in the order Ir > Pt > Ru > Rh⁴. Vast literature survey is available on the selective hydrogenation of α , β -unsaturated aldehydes catalyzed by different noble metals supported catalysts¹⁵⁻¹⁷. In addition catalytic hydrogenation of α , β -unsaturated aldehydes are mostly based on supported metals platinum based bimetallic catalysts¹⁸⁻³⁰. The selectivity towards unsaturated alcohols (geraniol and nerol) could also be increased by metal has deposited on reducible support as TiO₂, the hydrogenation of the C=O bond can be promoted due to the presence of partially reduced species generated upon reduction at high temperature, that is strong metal-support interaction (SMSI effect)³¹⁻³⁴ and also addition of second metals at the same phenomena. It has attracted much attention in noble metal supported on reduced oxides (SMSI) shows important differences in the catalytic activity and selectivity of hydrogenation reaction when reduced at high temperature, compared with one reduced at lower temperature or the corresponding noble metal supported on un-reducible supports (without SMSI). Most of the studies of SMSI concentrated on titania supported noble metal catalyst.

In this work, we report the preparation of titania supported bimetallic nanocatalyst by the impregnation method, being reduced in two different temperatures, 375 °C and 575 °C and characterised by BET surface area, FT-IR, XRD, SEM with EDAX, TEM and XPS techniques and their catalytic activity for selective hydrogenation of citral towards unsaturated alcohols (geraniol and nerol).

Experimental

The metal precursors H₂PtCl₆.6H₂O (0.1992 g in 10 mL water) and PdCl₂ (0.1250 g in 10 mL water), the both solutions were mixed together with stirring. The TiO₂ (9.85 g) in 50 mL water) dispersion was added to this solution with vigorous stirring and the resulting

suspension was aged at 80 °C for 24 h with stirring. An aqueous solution of NaBH₄ (0.4116 g in 10 mL water) was added drop wise into this suspension with vigorous stirring. The NaBH₄ aqueous solution was prepared in an ice bath and molar ratio of NaBH₄: (Pt and Pd) are 10:1. The prepared nanocatalysts denoted as Pt-Pd/TiO₂375 and Pt-Pd/TiO₂575. The above produce is used to synthesis Pt-Ru and Pt-Au nanocatalysts instead of using Pt-Pd.

BET surface area and X-ray diffraction (XRD)

The BET surface area measurements were made on a Micromeritics Gemini 2360 instrument by N₂ adsorption at liquid nitrogen temperature. Prior to measurements, samples were oven dried at 393 K for 12 h and flushed with argon gas for 2 h. X-ray diffraction (XRD) patterns have been recorded on a Siemens D-5000 diffractometer, using Ni-filtered Cu K_α (0.15418 nm) radiation source range of 20-90° was employed to determine phase of the modified TiO₂ powers. Crystalline phases were identified with the help of ASTM Powder Data Files.

Scanning electron microscopy (SEM) and Transmission electron microscopy (TEM)

The SEM analyses were carried out with a Jeol JSM 5410 microscope, operating with an accelerating voltage of 15 kV. Micrographs were taken after coating by gold sputtering. Elemental analysis was carried out on a KeveX, Sigma KS3 Energy dispersive X-ray (EDX) instrument operating at a detector resolution of 136 eV. TEM studies were carried out on a JEOL-JEM 100 electron microscope. Samples for direct examination were prepared by suspending the powder in ethanol and a drop of the suspension was allowed to dry on a copper grid coated with a carbon film. Extractive Replica was performed by ultrasonically dispersing the catalyst powder and depositing a drop of the suspension on freshly cleaved mica. After drying, the dispersed powder was covered by a carbon film. TEM (HRTEM) images were obtained by employing a JEOL-3010 device with 300 kV accelerating voltage.

X-ray photoelectron spectroscopy (XPS)

X-ray photoelectron spectroscopic (XPS) was used to analyze the atomic surface concentration on each catalyst. The spectra were recorded on a Perkin-Elmer model 5300 x-ray Photoelectron Spectrometer using Mg K_α-1253.6eV as a radiation source at 300W. The spectra were recorded in the fixed analyser transmission mode with pass energies of 89.32 and 35.61 eV for recording survey high resolution spectra, respectively. All binding energies were referenced to the C 1s peak at 284.6 eV, which is invariably present on the film surface. The spectra were fitted by XPSPEAK with a linear background and to 80%Gaussian/20% Lorentzian peak shape. The structure of anatase TiO₂ demonstrated in the manuscript was constructed by the Ca.R.Ine version 3.1 crystallography program package.

Activity test

Citral (mixture of E and Z forms, Merck, 99%) and isopropanol (Fluka, 99.5%) were used as received. The liquid phase citral hydrogenation experiments were performed in a stirred semi-batch reactor (model 4574, Parr Instrument Co.). Before the reaction the catalysts were reduced *in situ* under hydrogen (gas purity, 99.995%) flow (80-100 mL/min) for 2 h under 10MPa at 523 K. Then, the reactor was cooled to reaction temperature. Reactant mixture (200 mL of 0.1 M citral in isopropanol) was injected into the bubbling unit to remove the dissolved oxygen before it was injected into the reactor and contacted with the catalysts. Citral hydrogenation reaction was performed at 90 C, 10 MPa and at a stirring speed of 750 rpm. Preliminary runs carried out at different stirring rates, loading and catalysts grain size demonstrated the absence of internal and external transfer limitations under the selected conditions.

Results and Discussion

Physicochemical characterization

Surface area measurement

Figure 1 shows N_2 adsorption-desorption isotherm of that Pt-Pd/TiO₂, Pt-Ru/TiO₂ and Pt-Au/TiO₂ nanocatalysts. According to IUPAC nomenclature, all the isotherms are type IV classification isotherm³⁵. A sharp adsorption and desorption steps followed by a plateau at high P/P₀, which is characteristic of capillary condensation and evaporation in the pores, are clearly observed³⁶. While a hysteresis loop close to H₁-type is observed for the TiO₂ support. The hysteresis loop is changing with the noble metals incorporation. Then, evolution from H₁-type to H₂-type is observed (Figure 1). The absence of any sharp rise in the nitrogen uptake as P/P₀ close to 1 also tends to conclude on a homogeneous pore size repartition, without large pores in the support^{37,38}.

In addition, pore size (D_p) and pore volume (V_p) (Table 1) are decreased with the increase in reduction temperature of the prepared nanocatalysts. Further, the nanocatalyst exhibit decrease in surface area at higher temperature reduction than at lower temperature. The decrease of the pore volume is more marked as shown in Table 1.

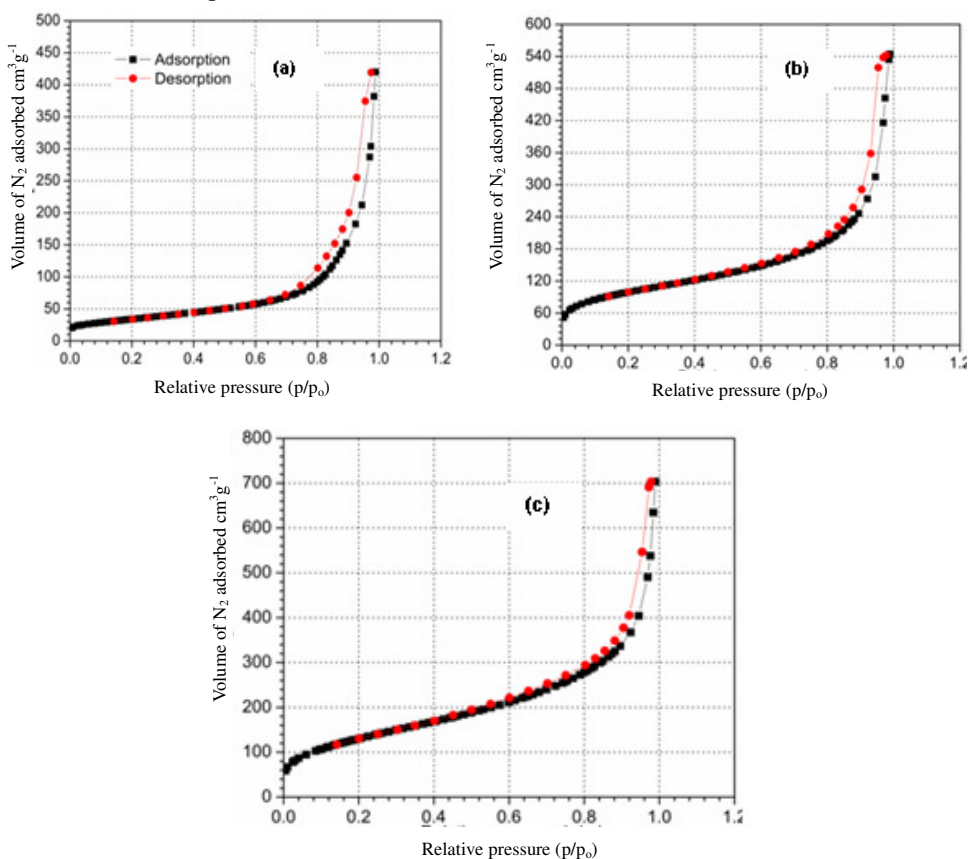


Figure 1. N_2 adsorption/desorption isotherm of bimetallic catalyst of (a) Pt-Pd/TiO₂ (b) Pt-Ru/TiO₂ and (c) Pt-Au/TiO₂ bimetallic catalyst

Table 1. N₂ adsorption-desorption measurements for TiO₂ supported bimetallic (Pt-Pd, Pt-Ru and Pt-Au) nanocatalysts

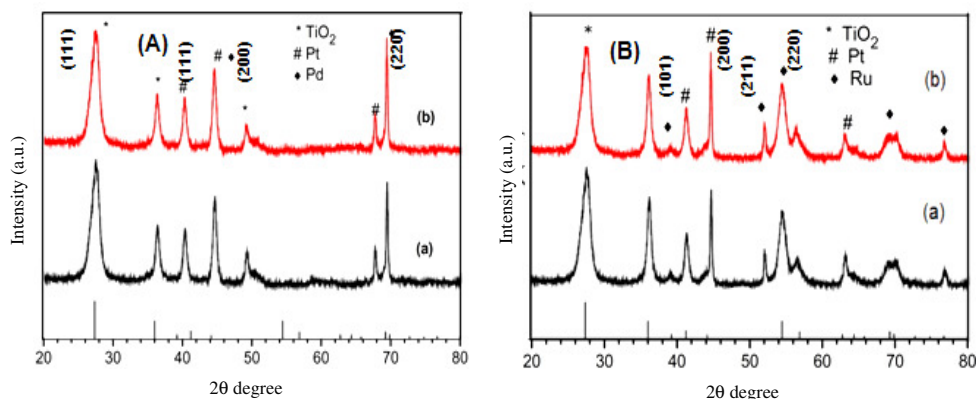
Nanocatalysts	Metal loading, mol % ^a				S _{BET} , m ² /g ^b	D _{pore} , nm ^c	V _{Pore} , cm ³ /g ^d
	Pt	Pd	Ru	Au			
Pt-Pd/TiO ₂ 375	0.8	0.7	-	-	46	18.1	0.27
Pt-Pd/TiO ₂ 575	0.9	0.6	-	-	44	20.3	0.22
Pt-Ru/TiO ₂ 375	0.8	-	0.7	-	49	17.4	0.21
Pt-Ru/TiO ₂ 575	0.7	-	0.8	-	45	21.2	0.15
Pt-Au/TiO ₂ 375	0.8	-	-	0.7	58	18.2	0.18
Pt-Au/TiO ₂ 575	0.9	-	-	0.7	53	19.8	0.17

^aICP method, ^bSpecific surface area deduced from the isothermal analysis at liquid nitrogen temperature in the relative pressure range from 0.05 to 1.00. ^cTotal pore volume. ^dPore diameter calculated using BJH method

XRD analysis

Powder XRD pattern of Pt-Pd/TiO₂375 and Pt-Pd/TiO₂575 nanocatalysts are given in Figure 2A, which exhibit diffraction peaks at 25.5°, 37.7° and 48.2° that are consistent with the (101), (004) and (200) is characteristic planes (JCPDS no.: 84-1286) of anatase TiO₂ [39,40] also exhibit other peaks at 39.9°, 46.3° and 67.45° with corresponding planes of (111), (200) and (220) is characteristic of Pt (JCPDS 04-802) and the peaks at 40.1°, 46.7° and 68.1° with corresponding planes of (111), (200) and (220) of Pd (JCPDS 05-0681) face centered phase.

Powder XRD pattern of Pt-Ru/TiO₂375 and Pt-Ru/TiO₂575 nanocatalysts are given in Figure 2B. In Figure 2B the diffraction peaks at 38.3°, 42.2°, 44.0°, 58.3°, 69.5° and 78.4° with corresponding to (100), (002), (101), (102), (110) planes is due to (JCPDS 06-0663) of hexagonal Ru. Furthermore, the diffraction peaks corresponding to Pt and TiO₂. Figure 2C shows that the powder XRD pattern of Pt-Au/TiO₂375 and Pt-Au/TiO₂575 nanocatalysts. The diffraction peaks 38.1°, 44.4°, 64.3° and 77.5° corresponding to (111), (200), (220), (311) and (112) planes are due to fcc phase (JCPDS card no. 06-0663) of Au. Further, the diffraction peaks corresponding Pt and TiO₂ is also found in Figure 2C.



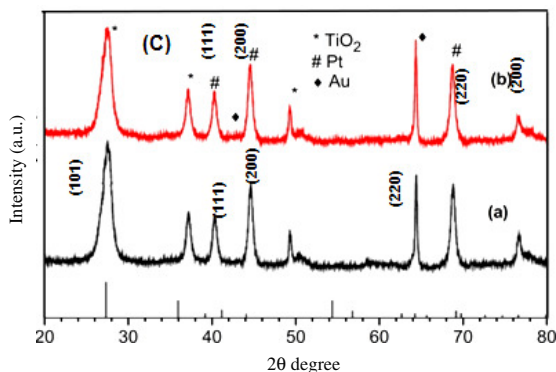


Figure 2. XRD pattern of (A) Pt-Pd/TiO₂, (B) Pt-Ru/TiO₂ and (C) Pd-Au/TiO₂ Nanocatalysts thermally reduced (a) 375 °C and (b) 575 °C

Scanning electron microscopy

The morphology of the synthesized nanocatalysts was investigated using SEM analysis. SEM images and the corresponding EDAX spectra of Pt-Pd/TiO₂, Pt-Ru/TiO₂ and Pt-Au/TiO₂, reduced at 575 °C are given in Figure 3 to 5 respectively. The micrographs show that the particles were spherical-like irregular particles with the average diameter is in nm range. For the nanocatalysts, reduced at higher temperature relatively larger particles are observed due to agglomeration at sintering process. The EDAX spectrum shows the presence of Pt, Pd, Au and Ru along with Ti and O.

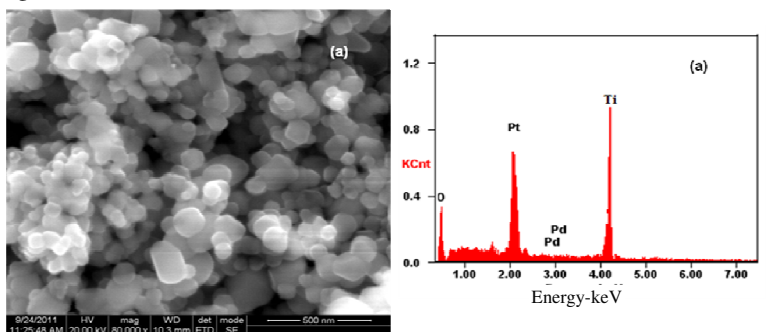


Figure 3. (a) SEM image of Pt-Pd/TiO₂575 (b) EDAX spectrum of Pt-Pd/TiO₂575

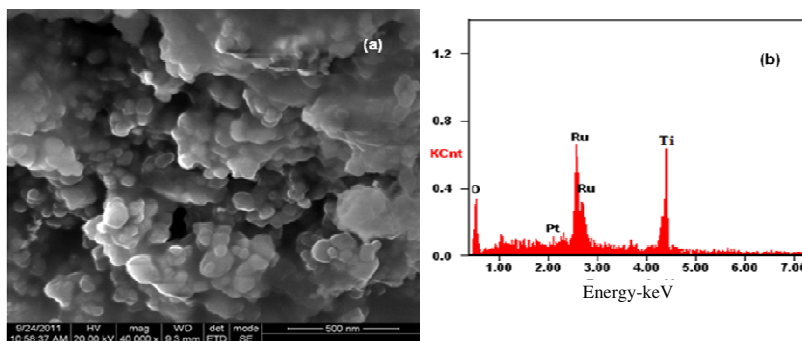


Figure 4. (a) SEM image of Pt-Ru/TiO₂575 (b) EDAX spectrum of Pt-Ru/TiO₂575

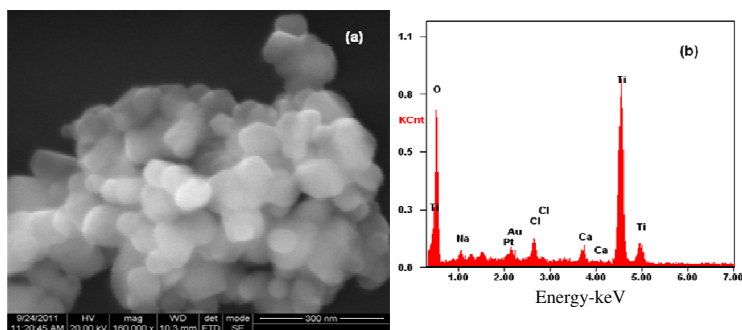


Figure 5. (a) SEM image of Pt-Au/TiO₂/575 (b) EDAX spectrum of Pt-Au/TiO₂/575

Transmission electron microscopy

The prepared nanocatalysts were subjected to TEM analysis to study the morphology of prepared samples. The TEM images and SAED pattern of the Pt-Pd/TiO₂ and Pt-Au/TiO₂ nanocatalysts thermally reduced at 375 and 575 °C are given in Figure 6 and 9 respectively. The morphology of samples was spherical and well dispersed and the sizes of the particles were in the range of 50-100 nm. It is observed that the catalysts reduced at 375 °C have smaller particle size than catalysts reduced at 575 °C. The SAED patterns show that the nanocatalysts are crystalline in nature. Reduction at higher temperatures lead to significant increase in size and agglomeration of nanoparticles at the exterior surface compared to the catalysts reduced at lower temperature. The high magnification HRTEM images reveal the presence of orderly crystallites in the particles.

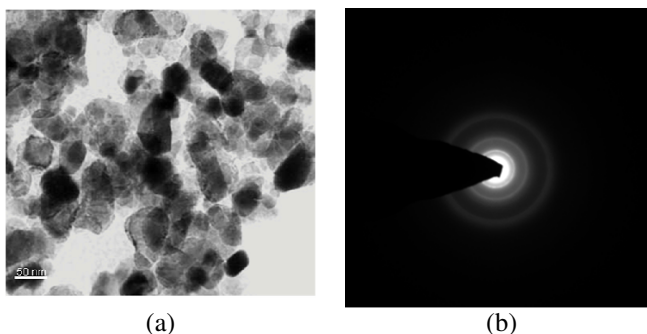


Figure 6: (a) TEM image (b) SAED pattern of Pt-Pd/TiO₂/375

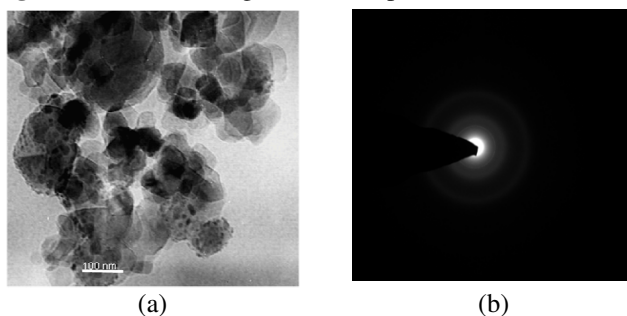


Figure 7 (a) TEM image (b) SAED pattern of Pt-Pd/TiO₂/575

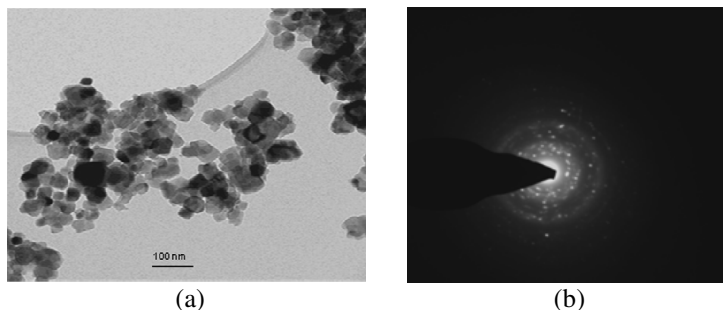


Figure 8. (a) TEM image (b) SAED pattern of Pt-Au/TiO₂/375

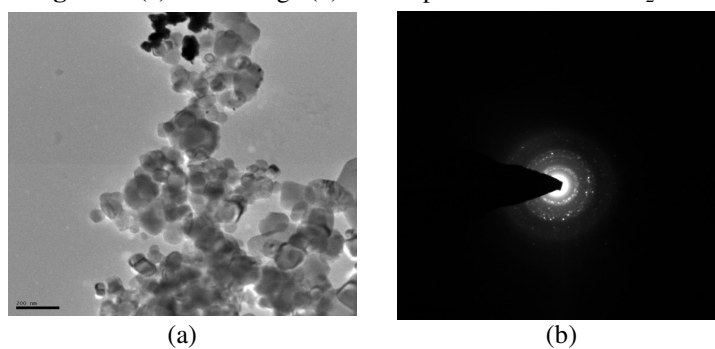


Figure 9. (a) TEM image (c) SAED pattern of Pt-Au/TiO₂/575

XPS of bimetallic supported on TiO₂ nanocatalysts

Figure 10 show the core level spectra of Ru 3d and Pt 4f of Pt-Ru/TiO₂/375 nanocatalyst. The core level spectrum of Ru 3d spectrum has been obscured by the C 1s (286.6 eV) spectrum, but the deconvoluted spectrum shows a doublet with peak binding energies of 282.29 eV (3d_{5/2}) and 286.286.1 eV (3d_{3/2}). It is difficult to resolve the small Ru peak from the large peak of C 1s. The Ru 3d spectra revealed the presence of only Ru⁰ at 3d_{5/2} at 282.32 eV⁴¹⁻⁴³.

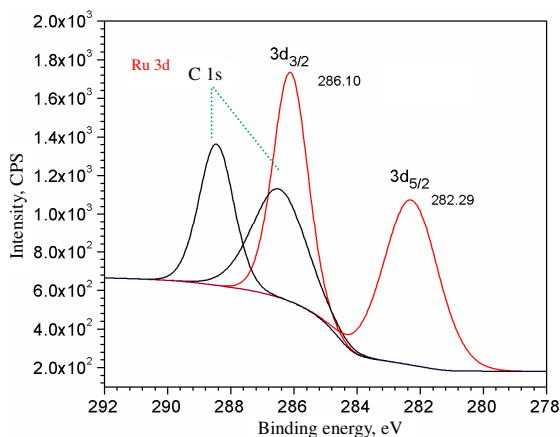


Figure 10. XPS Ru d 3d core level spectra of Pt-Ru/TiO₂ 375 °C

Nanocatalyst testing

Effect of second metal addition for higher selectivity of unsaturated alcohols

The Figure 11 shows, the unsaturated alcohols conversion and selectivity as a function of Pt-Pd/TiO₂, Pt-Ru/TiO₂ and Pt-Au/TiO₂ catalysts, thermally reduced at 375 °C and 575 °C. The catalysts reduced at low temperature (375 °C) shows the overall conversion and selectivity of GOL & NOL 48, 72 and 45% and 45,70 and 40% for bimetallic catalysts Pt-Pd/TiO₂, Pt-Ru/TiO₂ and Pt-Au/TiO₂ respectively, which is shown in Figure 11a. The catalysts thermally reduced at high temperature (575 °C) exhibit the overall conversion and selectivity of GOL & NOL 55, 78 and 53% and 52, 75 and 48% for bimetallic Pt-Pd/TiO₂, Pt-Ru/TiO₂ and Pt-Au/TiO₂ catalysts respectively, which is shown in Figure 11b. The catalysts reduced at 575 °C show higher activities than their counterparts reduced at 375 °C. This phenomenon is explained by the presence of partially reduced support species TiO_(2-x) generated after reduction at high temperature, which can cover part of the metallic surface⁴⁴⁻⁴⁷. The bimetallic catalysts relatively show higher activity than the monometallic catalysts, which may be due to the cooperative activity of the two metals⁴⁸⁻⁵³.

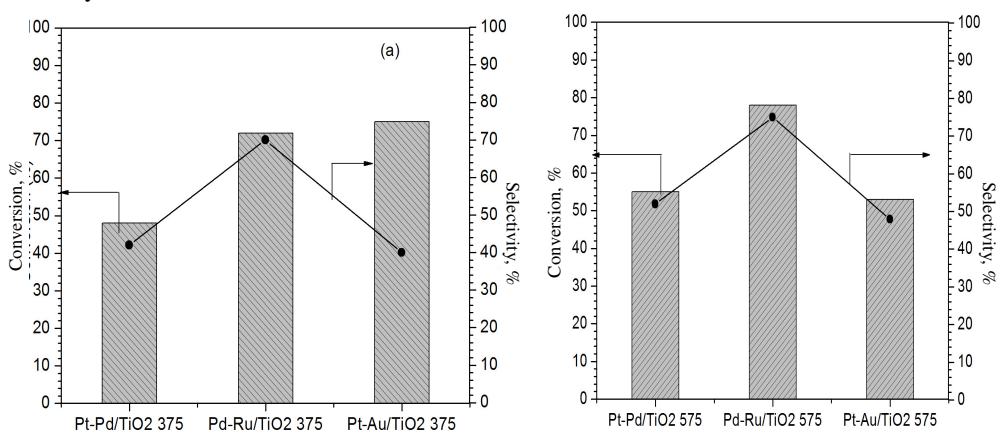
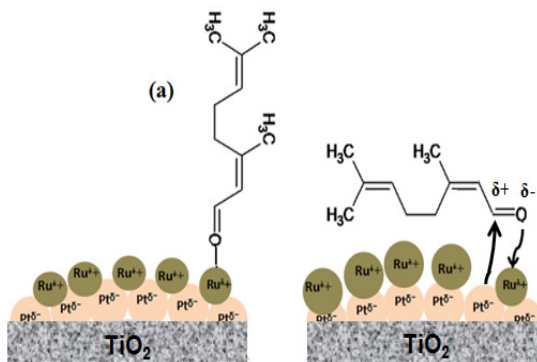


Figure 11. Conversion and selectivity towards unsaturated alcohols as a function of reduction temperature of catalyst (a) 375 and (b) 575 °C at 90 °C, 10 MPa, 750 rpm, IPA solvent, 1.5% metal content and m= 250 mg

Effects of ruthenium promoter on Pt catalysts

Among the prepared TiO₂ supported bimetallic (Pt-Pd/TiO₂ and Pt-Ru/TiO₂ and Pt-Au/TiO₂) nanocatalysts Pt-Ru/TiO₂ shows the highest overall conversion and selectivity towards GOL & NOL. The XPS analysis shows the presence of Pt⁰ and Ru⁰. In the Pt-Ru/TiO₂ nanocatalyst the contact between Pt and Ru atoms favors the partial electronic transfer from Ru⁰ towards Pt⁰ due the difference in electronegativity. In this way, there is + δ charge density in the Ru atoms and a - δ charge density in the Pt atoms (Scheme 2). Eventhough, Ru, Pd and Au have the same electronegativity; Ru is a hard acid, whereas Pd and Au are soft acids. Considering a molecule of α , β -unsaturated aldehyde, it is accepted that the C=O group could be adsorbed on to the Ru metal surface⁵² due to partial negative charge (- δ) on the O atom. Which favours the hydrogenation of the C=O group resulting in the formation of unsaturated alcohols. The mode of adsorption of citral over Pt-Ru/TiO₂ catalyst is shown in the Scheme 2.



Scheme 2. Adsorption mode of citral

Conclusion

The characterization techniques showed that the TiO₂ supported platinum based bimetallic nanocatalysts have a porous nature with high surface area and pore volume. The SMSI effect was evaluated by performing the hydrogenation on the catalysts, thermally reduced at low (375 °C) and high (575 °C) temperatures. The bimetallic nanocatalysts are able to generate reactive TiO_(2-x) species after reduction at high temperature (575 °C), leading to a SMSI effect comparable or superior to that on Pt-Ru supported on bulk titania. The SMSI effect shows that the catalysts reduced at higher temperature leads to an increase in selectivity toward unsaturated alcohols (GOL & GOL) for Pt-Ru/TiO₂ compared to Pt-Pd/TiO₂ and Pt-Au/TiO₂ nanocatalysts. In addition a second metal (Ru) also leads to an increase of the GOL & NOL selectivity during the citral hydrogenation. The generated partially oxidized second metal species due to the difference in electronegativity, strongly binds the C=O group and also paves the way for the selective activation of the C=O bond. Metal support interaction and promoter active metal interaction increased the unsaturated alcohol formation.

Reference

1. Claus P, *Top Catal.*, 1998, **5**, 51.
2. Smith G V and Notheisz F, *Heterogenous Catalysis in Organic Chemistry*, Academic Press, San Diego, 1999.
3. Gallezot P and Richard D, *Catal Rev Sci Eng.*, 1998, **40(1-2)**, 81-126.
4. Ponc V, *Appl Catal A*, 1997, **149**, 27.
5. Coq B, Figueras F, Geneste P, Moreau C, Moreau P and Warawdekar M, *J Mol Catal.*, 1993, **78**, 211.
6. Reyes P, Rojas H, Pecchi G and Fierro J L G, *J Mol Catal A*, 2002, **179(1-2)**, 293.
7. Mukherjee S and Albert Vannice M, *J Catal.*, 2006, **243(1)**, 108-130.
8. Alvarez-Rodriguez J, Gerrero-Ruiz A, Rodriguez-Ramos I and Arcoya-Martín A, *Microporous Mesoporous Mater.*, 2006, **97**, 122-131.
9. Vilella I M, Borbath I, Margitfalv J L, Lazar K, Miguel de O A and Scelza S R, *Appl Catal A*, 2007, **326**, 37.
10. Neri G, Milone C, Donato A, Mercadante L and Visco A M, *J Chem Tech Biotechnol.*, 1994, **60**, 83-88.
11. Serrano-Ruiz J C, Sepulveda-Escribano A, Rodriguez-Reinoso F and Duprez D, *J Mol Catal A*, 2007, **268**, 227.

12. Chiang S J, Yang H C, Chen Y Z and Liaw B J, *Appl Catal A Gen*, 2007, **326(2)**, 180.
13. Manikandan D, Divakar D and Sivakumar T, *Catal Lett.*, 2008, **123**, 107-114.
14. Galvagno S, Milone C, Neri G, Donato A and Pietropaolo R, *Stud Surf Sci Catal.* 1993, **78**, 163-170.
15. Centomo P, Zecca M, Lora S, Vitulli G, Caporusso A M, Tropeano M L, Milone C, Galvagno S and Corain B, *J Catal.*, 2005, **229(2)**, 283.
16. Neri G, Mercadante L, Donato A, Visco A M and Galvagno S, *Catal Lett.*, 1994, **29**, 379-386.
17. Burgener M, Furrer R, T. Mallat T and Baiker A, *Appl Catal A*, 2004, **268(1-2)**, 1-8.
18. Arvela P M, Tiainen L P, Neyestanaki A K, Sjöholm R, Rantakylä T K, Laine E, Salmi T and Murzin D Y, *Appl Catal A*, 2002, **237(1-2)**, 181-200.
19. Consonni M, Jokic D, Murzin D Y and Touroude R, *J Catal.*, 1999, **188**, 165-175.
20. Singh U K and Vannice M A, *J Catal.*, 2001, **199**, 73.
21. Malathi R and Viswanath R P, *Appl Catal A Gen*, 2001, **208**, 323-327.
22. Ammari F, Lamotte J and Touroude R, *J Catal.*, 2004, **221**, 32-42.
23. Abid M, Ehret G and Touroude R, *Appl Catal A*, 2001, **217**, 219.
24. Baeza B B, Rodríguez I R and Ruiz A G, *Appl Catal A*, 2001, **205(1-2)**, 227
25. Aumo J, Lilja J, Arvela A M, Salmi T, Sundell M, Vainio H and Murzin D Y, *Catal Lett.*, 2002, **84**, 219-224.
26. Silva A M, Santos O A A, Mendes M J, Jordão E and Fraga M A, *Appl Catal A*, 2003, **241**, 155-165.
27. Li Y, Li Z G and Zhou R X, *J Mol Catal A Chem.*, 2008, **279**, 140-146.
28. Reyes P, Aguirre M C, Fierro J L G, Santori G and Ferretti O, *J Mol Catal A Chem.*, 2002, **184**, 431-441.
29. Vilella I M J, de Miguel S R and Scelza O A, *J Mol Catal A Chem.*, 2008, **284**, 161-171.
30. Sordelli L, Psaro R, Vlaic G, Cepparo A, Recchia S, Dossi C, Fusi A and Zandoni R, *J Catal.*, 1999, **182**, 186.
31. Poondi D and Vannice M A, *J Mol Catal A Chem.*, 1997, **124**, 79.
32. Ekou T, Vicente A, Lafaye G, Especel C and Marecot P, *Appl Catal A Gen.*, 2006, **314**, 73-80.
33. Maki-Arvela P, Haćjek J, Salmi T and Yu Murzin D, *Appl Catal A Gen.*, 2005, 292, 1-49.
34. Ekou T, Ekou L, Vicente A, Lafaye G, Pronier S, Especel C and P. Marecot P, *J Mol Catal A Chem.*, 2011, **337**, 82-86.
35. Gregg S J and Sing K S, *Adsorption Surface Area and Porosity*, 2nd Ed., Academic Press, New York, 1982.
36. Margolese D, Melero J A, Christiansen S C, Chmelka B F and Stucky G D, *Chem Mater.*, 2000, **12**, 2448-2459.
37. Sen T, Tiddy G J T, Casci J L and Anderson M W, *Chem Commun.*, 2003, **9(17)**, 2182.
38. Zhu H, Jones D J, Zajac J, Dutartre R, Rhomari M and Roziere J, *Chem Mater.*, 2002, **14**, 4886-4894.
39. Mihailova B, Valtchev V, Mintova S and Konstantinov L, *Zeolites.*, 1996, **16(1)**, 22-24.
40. Lihitkar N B, Abyaneh M K, Samuel V, Pasricha R, Gosavi S W and Kulkarni S K, *J Collo Intet Sci.*, 2007, **314**, 310-316.
41. Rochefort D, Dabo P and Guay D, *Electrochimica Acta*, 2003, **48**, 4245-4252.
42. Aaltonen T, Alen P, Leskela M and Ritala M, *Chem Vap Depos.*, 2003, **9(1)**, 45-49.
43. Oh Y J, Moon S H and Chung C H, *J Electrochem Soc.*, 2001, **148(4)**, F56-F62.
44. Englisch M, Ranade V S and Lercher J A, *Appl Catal A: Gen.*, 1997, **163**, 111-122.

45. Reid R C, Prausnitz J M and Sherwood T K, *The Properties of Gases and Liquids*, McGraw Hill, New York, 1977.
46. Chesters M A, De La Cruz C, Gardner P, McCash E M, Pudney P, Shahid G and Sheppard N. *J Chem Soc Faraday Trans.*, 1990, **86**, 2757-2763.
47. Yoon C, Yang M N and Somorjai G A. *J Catal.*, 1998, **176**, 35-41.
48. Michael R Salata and Tobin J Marks, *Macromolecules*, 2009, **42**, 1920-1933.
49. Ismagilov Z R, Matus E V, Yakutova A M, Protasova L N, Ismagilov I Z, Kerzhentsev M A, Rebrov E V and Schouten J C, *Catal Today*, 2009, **147S**, S81-S86.
50. Rojas H, Borda G, Reyes P, Martínez J J, Valencia J and Fierro J L G, *Catal Today*, 2008, **133-135**, 699-705.
51. Ekou T, Vicente A, Lafaye G, Especel C and Marecot P, *Appl Catal A Gen.*, 2006, **314**, 73.
52. Protasova L N, Rebrov E V, Glazneva T S, Berenguer-Murcia A, Ismagilov Z R and Schouten J C, *J Catal.*, 2010, **271(2)**, 161-169.
53. Singh U K and Vannice M A, *J Mol Catal A Chem.*, 2000, **163**, 233-250.